Journal of Power Sources 230 (2013) 109–114

Contents lists available at SciVerse ScienceDirect

Journal of Power Sources

journal homepage: www.elsevier.com/locate/jpowsour

Short communication

Optimization of current collection to reduce the lateral conduction loss of thin-film-processed cathodes

Ho-Sung Noh [a], Jaeyeon Hwang [a,b], Kyungjoong Yoon [a], Byung-Kook Kim [a], Hae-Weon Lee [a], Jong-Ho Lee [a], Ji-Won Son [a,*]

[a] High-Temperature Energy Materials Research Center, Korea Institute of Science and Technology, Hwarangno 14-gil 5, Seongbuk-gu, Seoul 130-791, Republic of Korea
[b] Dept. of Materials Science and Engineering, Korea University, 145 Anam-ro, Seongbuk-gu, Seoul 136-701, Republic of Korea

HIGHLIGHTS

- We report optimization of the current collection for thin-film processed cathodes.
- The cell performance is improved by more than 30% by changing the MIC rib design.
- In all, the cell performance is improved by a factor of 1.6 than the original value.
- The power density at 0.7 V of 562 mW cm^{-2} at 600 °C is achieved.

GRAPHICAL ABSTRACT

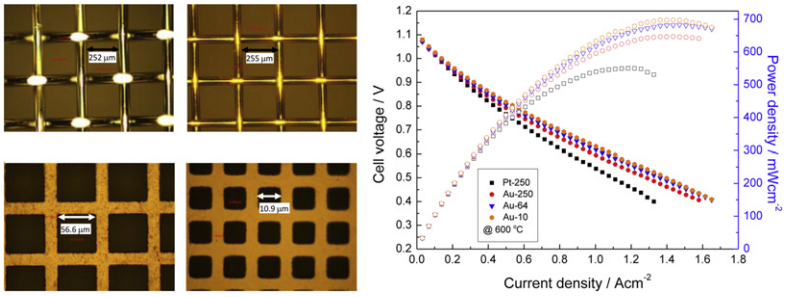

ARTICLE INFO

Article history:
Received 21 November 2012
Received in revised form
12 December 2012
Accepted 15 December 2012
Available online 22 December 2012

Keywords:
Thin-film-processed cathode
Solid-oxide fuel cell
Lateral conduction loss
Current collection
Contact material

ABSTRACT

To reduce the lateral conduction loss of thin-film-processed lanthanum strontium cobaltite (LSC) cathodes, the optimization of the current collection configuration is investigated. By increasing the number of the ribs in the metallic interconnects (MIC) and reducing the gap between the ribs, the lateral conduction distance at the cathode can be decreased, and as a result, cell performance can be improved by more than 30%. In addition, by changing the contact material from platinum to more resilient gold, the ohmic area specific resistance (ASR) is significantly reduced by the increase in effective contact area due to the deformation of the gold mesh. Furthermore, when a gold mesh with a finer grid size is used, the polarization ASR is decreased as well because the charge drainage can be improved by the enhanced current collection. With the optimization of the current collection, the cell performance is improved by a factor of 1.6 in comparison with that of the original test configuration. A power density of 562 mW cm^{-2} at 0.7 V and 600 °C is obtained with only approximately 2-μm-thick LSC cathodes.

1. Introduction

Recently, thin-film-processed cathodes fabricated by using techniques such as pulsed laser deposition (PLD) [1,2], sputtering [3–5], and solution spin-on [6,7] have been actively studied and employed in achieving high performance in low- and intermediate-temperature (LT and IT) operating solid-oxide fuel cells (SOFCs). The nano-porous and nano-crystalline nature of thin-film-processed cathodes is expected to increase the surface area and the number of reaction sites, which would yield higher performance than that of a conventional powder-processed cathode [1,8]. In addition, because thin-film-processed cathodes are fabricated at much lower processing temperatures than cathodes produced by powder processing, the reaction between high-performance cathode materials, such as lanthanum strontium cobaltite (LSC) and lanthanum strontium cobalt ferrite (LSCF), and zirconia-based electrolytes can be prevented [1,2,7,9].

* Corresponding author. Tel.: +82 2 958 5530; fax: +82 2 958 5529.
E-mail addresses: jwson@kist.re.kr, jiwon.son@gmail.com (J.-W. Son).

0378-7753/$ – see front matter © 2012 Elsevier B.V. All rights reserved.
http://dx.doi.org/10.1016/j.jpowsour.2012.12.059

In general, the method used to obtain a thin-film-deposited cathode with nano-porous structure is to deposit a film of low density at room temperature and high ambient processing pressure, then elevate the temperature to induce agglomeration, dewetting, and/or crystallization [1,3–5,9–11]. By this approach, crack-like vertical pores are generated in thin-film-processed electrodes due to the constrained shrinkage of the electrode film [1,3,5,12]. Due to the vertical pores that separate the cathode domain, as well as the thinness of the thin-film cathode, lateral conduction in the thin-film-processed cathode is substantially limited relative to that in conventional cathodes. This limited lateral conduction could be a significant problem when attempting to connect unit cells.

Due to the geometry of the thin-film deposition, it is more common for a thin-film-processed cathode to be employed in a planar SOFC. In planar SOFCs, metallic interconnects (MICs) are generally used to connect the cells in the stack. If the lateral conduction is limited and thus the current collection is ineffective, a significant area specific resistance (ASR) loss occurs due to the contact problem between the electrode and the MIC [13–16]. In conventional SOFCs with a substantially thick (~several tens of microns) powder-processed cathode, the loss can be significantly reduced by inserting contact materials, such as Pt, Au, or Ag meshes, between the MIC and the cathode [14,15]. For example, for an anode-supported SOFC with an 8-μm-thick yttria-stabilized zirconia (YSZ) electrolyte, a sputtered gadolinia-doped ceria (GDC) buffer layer, and a screen-printed ~30-μm-thick LSC-GDC composite cathode, the ohmic ASR of the cell is only approximately 6 (~6%) and 5 mΩ cm^2 (~2.5%) higher than the calculated ASR of the YSZ electrolyte at 650 and 600 °C, respectively, when a Pt mesh is inserted as a contact material [17].

This method is, however, insufficient for the effective current collection of thin-film-processed cathodes. Although MICs with Pt meshes have been employed for current collection, the ohmic ASR of a YSZ-based cell with a 3-μm thin-film LSC cathode is approximately 160 mΩ cm^2, which is more than twice the calculated ASR of a 6-μm-thick YSZ/200-nm-thick GDC electrolyte (~67 mΩ cm^2) at 650 °C [1]. For cells with a much smaller electrolyte ASR, ineffective current collection becomes more serious. For a thin-film electrolyte SOFC featuring a 200-nm-thick YSZ/1-μm-thick GDC bilayer electrolyte, the measured cell ohmic ASR is more than five times higher than the electrolyte ASR [18]. This significant loss from sources other than the cell itself may hamper the investigation of the true effect of variation in cell components, such as variation in materials, microstructure, dimensions, etc. In fact, the effect of the thickness of an ultra-thin YSZ blocking layer was not reflected in the measured cell performance in a previous study by the authors [18].

Therefore, in this study, several methods for reducing lateral conduction loss by changing the cell testing configuration were employed and the effect of these variations on the measured cell performance was investigated. Identical anode-supported SOFCs with LSC thin-film cathodes were subjected to various test configurations. First, the rib design of the MIC was changed to reduce the distance between the ribs. Second, the contact mesh material and the grid size of the mesh were varied to investigate the effect of the direct-contact area over the thin-film cathode. The ASR values and power outputs of the modified cells were compared with those of the cell in the original configuration.

2. Experimental

Half cells measuring 2 cm by 2 cm with an approximately 6-μm-thick YSZ electrolyte over a NiO-YSZ anode support were diced from a 10 cm by 10 cm cell. Because all of the tested cells were derived from a single cell, it can be assumed that the properties of the cells, including the dimensions of the components of the cells up to the YSZ electrolyte, were similar. The whole surface of the YSZ electrolyte was covered with a ~200-nm-thick GDC fabricated by PLD. The GDC layer was deposited at a substrate temperature (T_s) of 700 °C and ambient oxygen pressure (P_{amb}) of 6.67 Pa. An

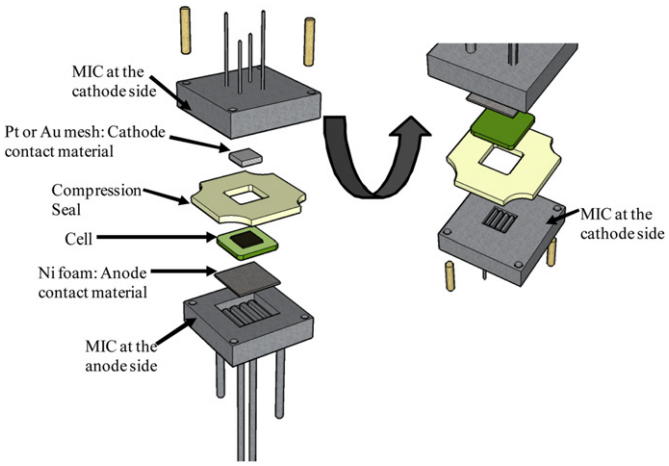

Fig. 1. Cell test configuration used in this study.

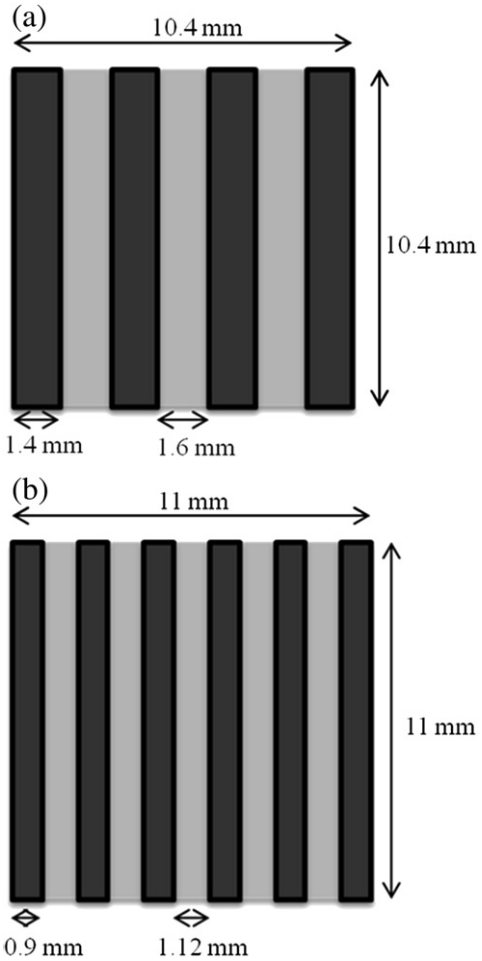

Fig. 2. Cathode-side MIC rib designs. (a) Original configuration and (b) modified configuration.

approximately 2-μm-thick LSC layer was deposited on the GDC layer at room temperature and at a P_{amb} of 13.3 Pa. The thickness of the cathode was determined to prevent cathode/electrolyte delamination [1]. The cell was subjected to post-annealing at 650 °C for 1 h to induce the crystallization and porous microstructure of the cathode.

Fig. 1 provides an illustration of the cell test configuration. A cell, a nickel foam as the anode contact, a noble-metal mesh as the cathode contact, and a ceramic-glass composite-based composite seal [19] were placed between the MICs. A mechanical load for contact and sealing was applied for testing. Air and humidified H_2 (3% H_2O) were used as the oxidant and the fuel, respectively, and the flow rates of each side were held constant at 200 sccm. The cell operation temperature was varied from 650 to 500 °C at intervals of 50 °C, and electrochemical impedance spectra (EIS)under the open-circuit voltage (OCV) condition and current–voltage–power (*I–V–P*) curves were obtained at each temperature. To prevent the degradation of the cathode, which was post-annealed at 650 °C, the first cell-performance measurement was conducted at 600 °C; then, the measurement temperature was reduced to 500 °C. The performance at 650 °C was tested as the last measurement. In this article, therefore, the performance measured at 600 °C will be primarily referenced because it reflects the performance that was initially measured and less affected by any possible degradation of the thin-film cathode during the cell test. A Solartron impedance analyzer with an electrochemical interface (SI1260 and SI1287) was used to obtain EIS and *I–V–P* curves, and each EIS was observed over a frequency range from 10 MHz to 0.1 Hz. The AC amplitude of the impedance measurements was 50 mV. After the cell test, the microstructures of each cell were characterized by using scanning electron microscopy (SEM, XL-30, FEI). The cell fabrication and measurement methods were based on previous studies [1,9,20].

To investigate the effect of the change in the rib design at the MIC, two cathode rib designs were compared, the original rib design consistently used in the previous study [1,9,18,20] and the modified rib design. In the modified rib design, the total number of ribs was increased and the gap between the ribs was reduced. The original rib design on the cathode side is shown in Fig. 2(a). Four 1.4-mm-wide ribs separated by 1.6-mm gaps are shown over an area measuring 10.4 mm by 10.4 mm. The modified rib design is shown in Fig. 2(b). Six 0.9-mm-wide ribs separated by 1.12-mm gaps are shown over an area measuring 11 mm by 11 mm.

To vary the cathode contact mesh type, four different meshes were tested. The Pt meshes (Tanaka Precious Metals, Japan) used in the original cell test, with openings measuring 250 μm by 250 μm (Pt-250), were employed in the rib design comparison experiment. Au meshes with openings measuring 250 μm by 250 μm (Au-250), 64 μm by 64 μm (Au-64), and 10 μm by 10 μm (Au-10) (Good fellow Cambridge Ltd., UK) were used to investigate the effect of the variation in contact material and grid size. Optical micrographs of each mesh are shown in Fig. 3. The Pt-250 and Au-250 meshes are wire-weaved, and the other two are patterned. Several layers of meshes were laminated for handling and used as the contact material on the cathode side.

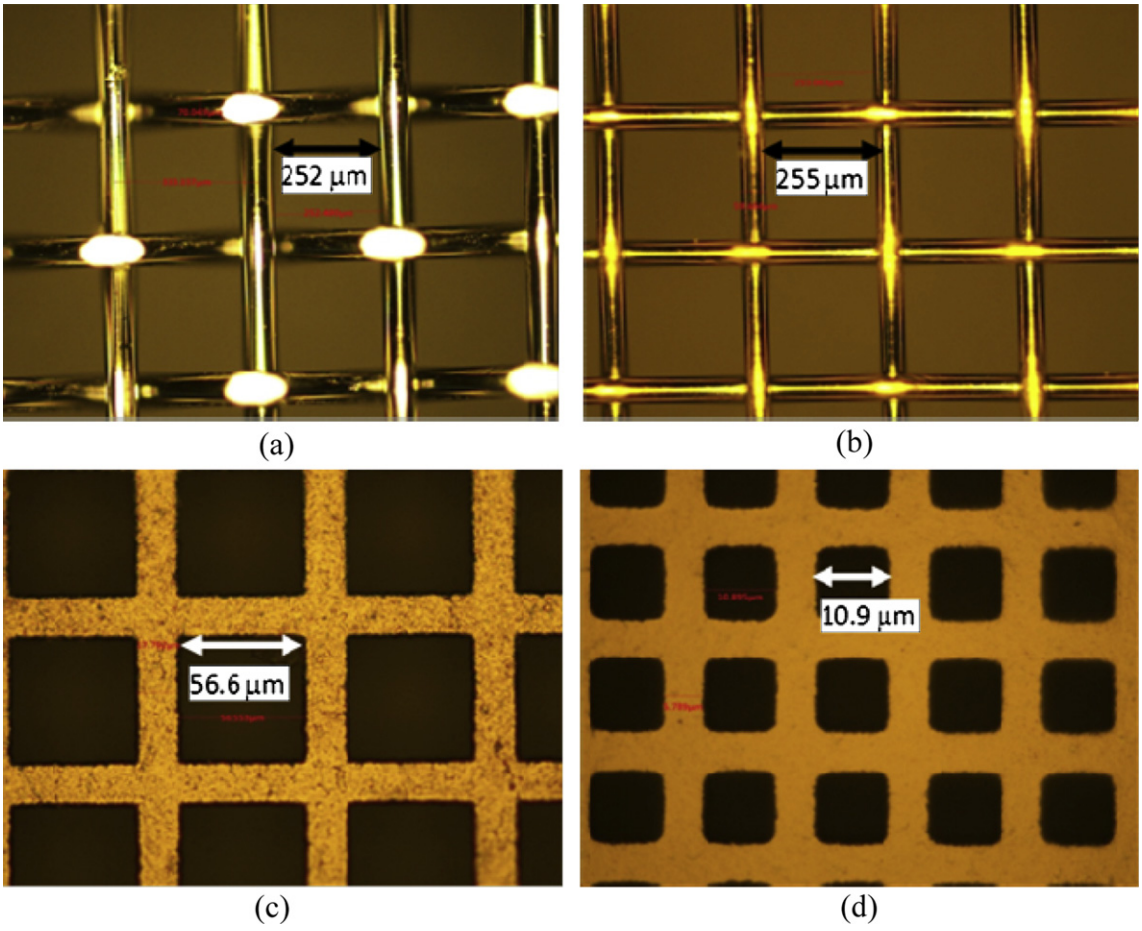

Fig. 3. Optical micrographs of the meshes used as the cathode contact material: (a) Pt-250, (b) Au-250, (c) Au-64, and (d) Au-10.

3. Results and discussion

Fig. 4 shows surface and cross-sectional SEM micrographs of the tested cell. As was reported before [1,9,20], a chasm-like separation of the cathode domains was developed in the thin-film LSC cathode. The chasm-like separation reaches the interface between the cathode and the GDC surface, as shown in the cross-section of the cell (Fig. 4(b)). The cross-sectional microstructure shows that the dimensions of the LSC cathode, GDC buffer, and YSZ electrolyte are ~2 μm, 200 nm, and 6 μm, respectively. It was confirmed that all of the cells tested in this study had almost identical component dimensions, which indicates that any difference in performance between the cells does not originate from the cells themselves.

First, the effect of changing the rib design at the cathode MIC was investigated. Fig. 5(a) compares the *I–V–P* curves (measured at 600 °C) of the cells tested in each setup with the rib designs shown in Fig. 2. By changing the rib design, the peak power density increased by 131 mW cm^{-2} (420–551 mW cm^{-2}) and the power density at 0.7 V increased by 109 mW cm^{-2} (332–441 mW cm^{-2}), which represents an improvement in cell performance of more than 30%. Considering that the total contact area of the old setup (Fig. 2(a)) and that of the new setup (Fig. 2(b)) are 58.24 $cm^2$and

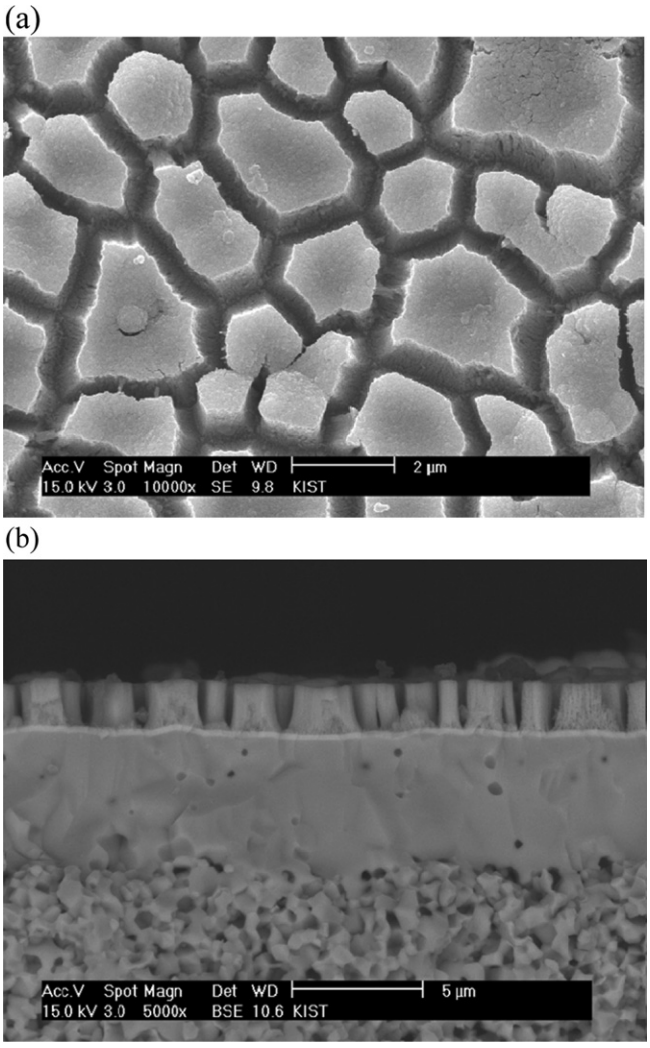

Fig. 4. (a) Surface of a thin-film LSC cathode over the electrolyte of a tested cell and (b) cross-sectional microstructure of a tested cell.

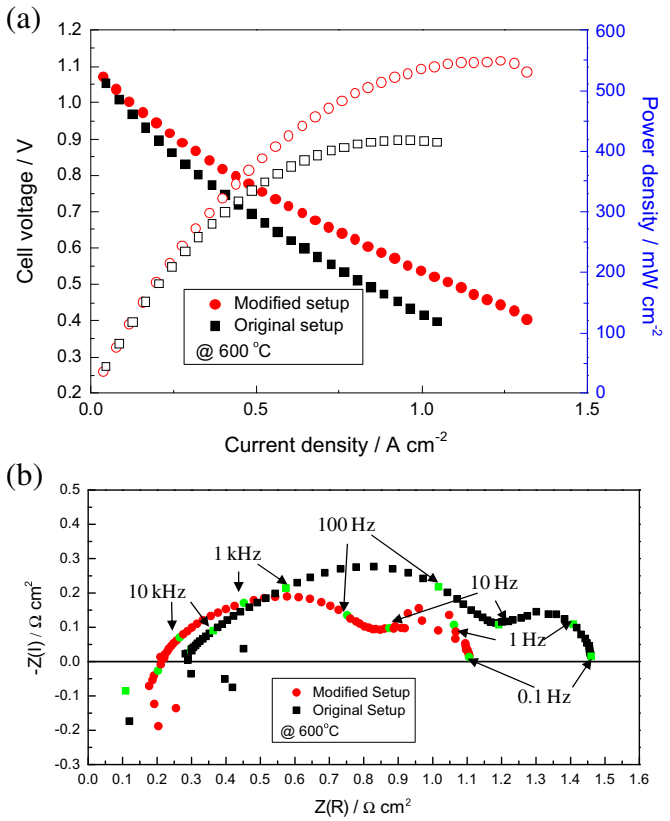

Fig. 5. (a) *I–V–P* curves and (b) EIS at OCV from the original and modified setups. The measurement temperature was 600 °C.

59.4 cm^2, respectively, which is only about a 2% difference, the improvement in cell performance observed by changing the rib design is quite significant. In Fig. 5(b), the EIS at the OCV of two measurements are compared. Both EIS have a similar shape. The ohmic ASR was reduced from 0.290 to 0.210 Ω cm^2, and the polarization (pol.) ASR was reduced from 1.170 to 0.896 Ω cm^2. The ASRs were reduced to 72.4% and 76.6% of their original values, respectively. Because the difference in contact area is not substantial, it is postulated that the major reason for the decrease in the ASR is the reduction in the gap between the ribs and the increase in the number of ribs, which reduces the lateral conduction distance for current collection.

Still, the measured ohmic ASR value is significantly higher than the calculated ASR value of the electrolyte. At 600 °C, the calculated ASR value of the 6-μm-thick YSZ/200 nm-thick GDC is 0.137 Ω cm^2, which is 65% of the measured ASR value in the modified setup. As mentioned previously, when the same setup was used for the powder-processed cathode [17], the electrolyte ASR was 95% of the measured ohmic ASR. This implies that a more efficient current collection configuration is necessary to compensate for the lateral conduction loss in the thin-film cathode. Because it is not possible to infinitesimally reduce the gap between the ribs, due to the limitations posed by the gas flow and the machining of the MIC, the contact mesh was varied to further assist lateral conduction.

In Fig. 6, the *I–V–P* curves and EIS of each cell measured with different meshes are compared. It is shown that the performance of the cell is improved by changing the mesh material and grid size (Fig. 6(a)). Interestingly, the greatest improvement was obtained when the mesh material was changed from Pt to Au. The peak power density was improved by 97 mW cm^{-2} (551 to 648 mW cm^{-2})

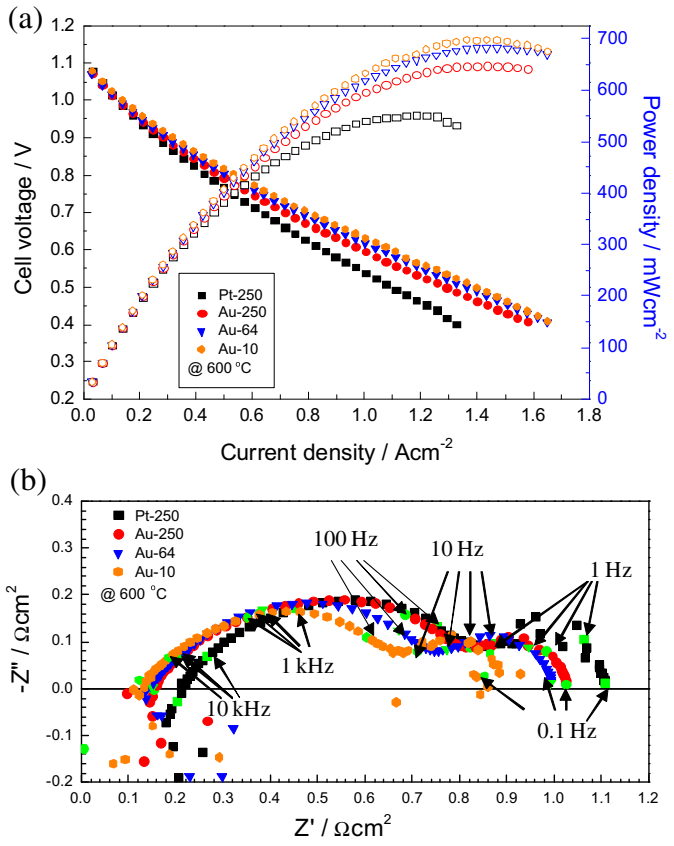

Fig. 6. (a) *I–V–P* curves and (b) EIS at OCV from the modified setup using different contact materials. The measurement temperature was 600 °C.

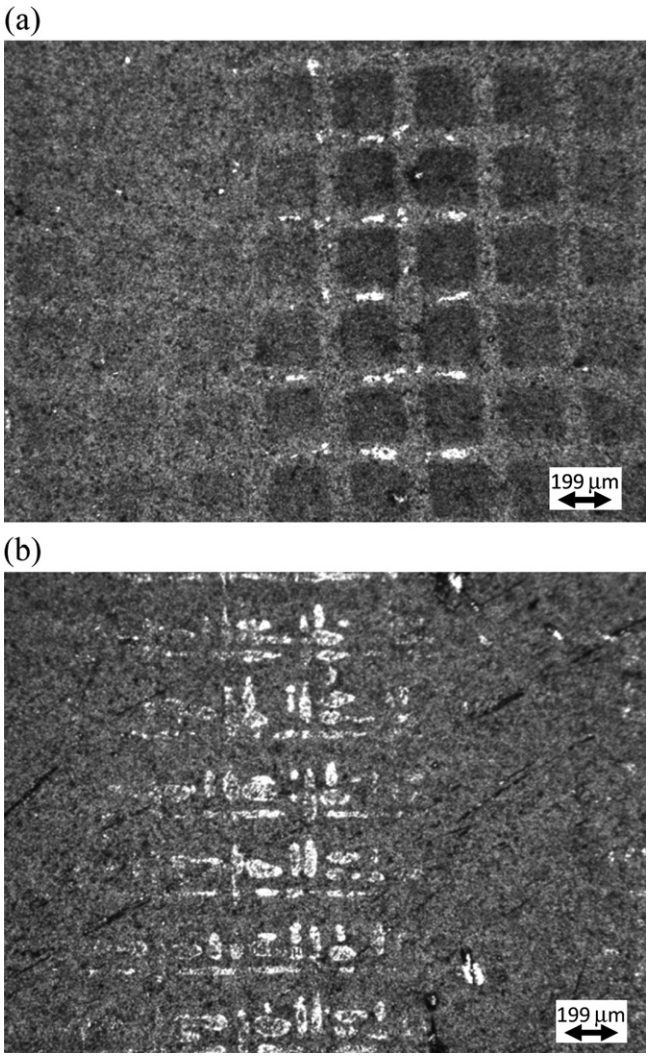

Fig. 7. Optical micrographs of contact material imprint patterns over the thin-film LSC cathodes. (a) Pt-250 and (b) Au-250.

and the power density at 0.7 V was improved by 59 mW cm^{-2} (441 to 500 mW cm^{-2}) when the Au-250 mesh was substituted for the Pt-250 mesh. The mesh size also affected the cell performance, with differences observed among cells featuring Au-250, Au-64, and Au-10 meshes, but the variation in performance was not as significant as that observed when changing the mesh material. In Fig. 6(b), the EIS are compared. As the mesh material was changed from Pt to Au, there was a significant reduction in the ohmic ASR. The change in the size of the Au mesh affected the ohmic ASR as well; however, the variation in the ASR was not as significant as that observed when the mesh material was changed, like the cell performance.

In terms of the ohmic ASR, it is believed that the ductility of Au provided better contact to the cathode surface. In Fig. 7, optical micrographs of the mesh imprint over the thin-film cathode are compared for Pt-250 and Au-250. In the case in which Pt-250 was used, the mesh imprint reflects the first layer that directly contacts the surface of the thin-film cathode. On the other hand, the Au-250 imprint shows the wire pattern from a layer other than the first. In addition, the Au-250 contact pattern shows that the Au wire in the mesh was deformed and the contact area enlarged by the deformation. Owing to the ductile nature of Au, the contact of the upper layer of the mesh and the deformation of the wire in Au-250 can increase the contact area and reduce the lateral conduction loss of the cell relative to the Pt-250-based system.

The results indicate that the decrease in the size of the Au meshes reduced the pol. ASR. Fig. 6(b) shows that the frequency range from 10 Hz to 10 kHz in particular is affected by the variation in mesh size. This frequency range is related to oxygen surface exchange according to our previous analysis [20]. When the current collection is improved, the surface exchange reaction can be enhanced because the produced electronic charges can be drawn more effectively. Therefore, the optimization and improvement of the current collection is important for both the ohmic and pol. ASRs.

In Table 1, the ASR values measured at the OCV and the power densities of the tested cells are listed. All measurements were made at 600 °C. The calculated ASR value of the 6-μm-thick YSZ/200 nm-thick GDC electrolyte is also listed for comparison. As the current collection configuration at the cathode is refined, the ohmic ASR is reduced, approaching values close to the electrolyte ASR value. A reduction in the pol. ASR is clearly shown as well. By mitigating the lateral conduction loss at the thin-film cathode, the cell performance was improved by more than 200 mW cm^{-2} (original/Pt-250 vs. modified/Au-10). By optimizing the current collection design and contact materials, only ~2-μm-thick thin-film cathodes can yield cell performance comparable or superior to ~30-μm-thick powder-processed cathodes, which again proves the effectiveness of employing nano-structured thin-film cathodes. The results demonstrate the importance of current collection design and contact materials in using thin-film-processed cathodes to fully exploit the merits of employing nano-structured thin-film cathodes.

Table 1
ASR values (measured at OCV) and power densities from different cell test configurations (at 600 °C).

Cell test configuration (Setup/Mesh)	Ohm. ASR at OCV (Ωcm^2)	Pol. ASR at OCV (Ωcm^2)	Power density at 0.7 V (mW cm^{-2})	Peak power density (mW cm^{-2})
Original/Pt-250	0.290	1.170	332	420
Modified/Pt-250	0.210	0.896	441	551
Modified/Au-250	0.158	0.866	500	648
Modified/Au-64	0.147	0.846	534	683
Modified/Au-10	0.134	0.749	562	698
Calculated electrolyte ASR (6 μm YSZ/200 nm GDC)	0.137	–	–	–
Performance of cell w/Powder-processed LSC-based cathode [17]	–	–	531	595

4. Conclusions

By optimizing the current collection configuration, the lateral conduction loss in a thin-film-processed cathode is effectively reduced. Modifying the rib design at the MIC to reduce the lateral conduction distance improves cell performance by more than 30%. Moreover, changing the contact material from Pt to more resilient Au improves the cathode/contact material/MIC contact, thus significantly reducing the ohmic ASR. Reducing the grid size further improves the current collection; thus, the pol. ASR is also reduced. By optimizing current collection, cell performance is improved by a factor of 1.6. The results indicate that effective current collection configuration is of the utmost importance in taking full advantage of thin-film-processed cathodes.

Acknowledgments

This work was supported by the Young Fellow Program of the Korea Institute of Science and Technology (KIST) and the Global Frontier R&D Program on Center for Multiscale Energy System (2011-0031579) through a National Research Foundation (NRF) grant funded by the Ministry of Education, Science and Technology (MEST), the Republic of Korea.

References

[1] H.-S. Noh, H. Lee, H.-I. Ji, H.-W. Lee, J.-H. Lee, J.-W. Son, J. Electrochem. Soc. 158 (2011) B1–B4.
[2] P. Plonczak, A. Bieberle-Hütter, M. Søgaard, T. Ryll, J. Martynczuk, P.V. Hendriksen, L.J. Gauckler, Adv. Funct. Mater. 21 (2011) 2764–2775.
[3] T. Ryll, H. Galinski, L. Schlagenhauf, P. Elser, J.L.M. Rupp, A. Bieberle-Hutter, L.J. Gauckler, Adv. Funct. Mater. 21 (2011) 565–572.
[4] C.-W. Kwon, J.-I. Lee, K.-B. Kim, H.-W. Lee, J.-H. Lee, J.-W. Son, J. Power Sources 210 (2012) 178–183.
[5] K. Kerman, B.-K. Lai, S. Ramanathan, J. Power Sources 196 (2011) 2608–2614.
[6] E.-O. Oh, C.-M. Whang, Y.-R. Lee, S.-Y. Park, D.H. Prasad, K.J. Yoon, J.-W. Son, J.-H. Lee, H.-W. Lee, Adv. Mater. 24 (2012) 3373–3377.
[7] C. Peters, A. Weber, E. Ivers-Tiffee, J. Electrochem. Soc. 155 (2008) B730–B737.
[8] L. Dieterle, D. Bach, R. Schneider, H. Stormer, D. Gerthsen, U. Guntow, E. Ivers-Tiffee, A. Weber, C. Peters, H. Yokokawa, J. Mater. Sci. 43 (2008) 3135–3143.
[9] H.-S. Noh, J.-W. Son, H. Lee, J.-S. Park, H.-W. Lee, J.-H. Lee, Fuel Cells 10 (2010) 1057–1065.
[10] H. Huang, M. Nakamura, P.C. Su, R. Fasching, Y. Saito, F.B. Prinz, J. Electrochem. Soc. 154 (2007) B20–B24.
[11] X. Chen, N.J. Wu, D.L. Ritums, A. Ignatiev, Thin Solid Films 342 (1999) 61–66.
[12] H.-S. Noh, J.-W. Son, H. Lee, H.-S. Song, H.-W. Lee, J.-H. Lee, J. Electrochem. Soc. 156 (2009) B1484–B1490.
[13] N.Q. Minh, J. Kor, Ceram. Soc. 47 (2010) 1–7.
[14] S.P. Jiang, J.G. Love, L. Apateanu, Solid State Ionics 160 (2003) 15–26.
[15] M. Kornely, A. Leonide, A. Weber, E. Ivers-Tiffée, J. Power Sources 196 (2011) 7209–7216.
[16] W. Kong, J. Li, S. Liu, Z. Lin, J. Power Sources 204 (2012) 106–115.
[17] H.Y. Jung, Hierachical Control of Nano-Composite Cathode for the Performance Improvement of Intermediate Temperature Solid Oxide Fuel Cell, Ph.D. thesis in Dept. Materials Science and Engineering, Seoul National University, Seoul, 2011.
[18] D.-H. Myung, J. Hong, K. Yoon, B.-K. Kim, H.-W. Lee, J.-H. Lee, J.-W. Son, J. Power Sources 206 (2012) 91–96.
[19] J.-H. Lee, H. Kim, S.M. Kim, T.-W. Noh, H.-Y. Jung, H.-Y. Lim, H.-G. Jung, J.-W. Son, H.-R. Kim, B.-K. Kim, H.-J. Je, J.-C. Lee, H. Song, H.-W. Lee, Adv. Energy Mater. 2 (2012) 461–468.
[20] J. Hwang, H. Lee, K.J. Yoon, H.-W. Lee, B.-K. Kim, J.-H. Lee, J.-W. Son, J. Electrochem. Soc. 159 (2012) F639–F643.